Melting and Generation of Micro-protrusions on Cathode Surface during Spark Conditioning Process in Vacuum

N. Kita, F. Kondo, H. Kojima and **N. Hayakawa**
Nagoya University
Furo-cho, Chikusa-ku
Nagoya 464-8603, Japan

H. Fukuda and **K. Yamamura**
MEIDENSHA CORPORATION
515 Kaminakamizo, Higashimakado
Numazu 410-8588, Japan

ABSTRACT

Spark conditioning is an effective method to increase the dielectric strength in vacuum by melting and removing micro-protrusions on the cathode surface. We aim to optimize the conditioning effect in vacuum for the application of vacuum circuit breakers (VCBs) to higher voltage levels. To obtain high breakdown (BD) voltage, the control of BD charge in the conditioning process is required. When a BD occurs, we have suggested that micro-protrusions can be generated on the cathode surface by particles from the anode. For the suitable control of BD charge, the meltability of generated micro-protrusions and their size are important. In this paper, we focus on the generation of micro-protrusions on the cathode surface in conditioning process. First, we conduct spark conditioning by repetitive impulse voltages of rod-plane electrodes made of OFHC Cu in a vacuum chamber with different BD charge. After that, we observe the surface of rod cathode with a digital microscope in order to count the number of visible protrusions and measure their radii. By considering the meltability of micro-protrusions, we quantitatively reveal the existence of residual protrusions that cannot be completely melted by BD. Next, we estimate the maximum size of generated micro-protrusions by BD charge. In consideration of the collision of ions into the anode accelerated by the anode sheath voltage, we estimate the meltable amount of anode material by the BD charge. We confirm that the radii of experimentally measured protrusions are close to the estimated ones. Moreover, we consider the difference in dielectric strength due to the difference in the initial surface condition of the electrodes. We clarify that the dielectric strength is improved by applying acid wash and heat treatment to the electrodes before conditioning, which can be optimized by the BD charge and the initial surface condition of the electrode.

Index Terms — **Vacuum discharge, conditioning, vacuum circuit breakers, vacuum interrupters, breakdown, micro-protrusion.**

1 INTRODUCTION

VACUUM circuit breakers (VCBs) and vacuum interrupters (VIs) have been widely used in medium voltage systems in recent years. They are expected to be used for higher voltage applications because of their high dielectric strength, high current interruption performance, easy maintenance, and environmental friendliness [1-3]. Basically, the vacuum breakdown (BD) is influenced by field emission on the cathode surface. Especially, micro-protrusions on the cathode negatively influence the BD process, because they locally and highly enhance the electric field strength on the cathode surface. In vacuum electrical insulation, spark conditioning is used to improve the dielectric strength. Especially, BD charge that is considered to contribute to the melting of electrode is important factor to determine the BD voltage after conditioning saturation. We have previously found that the BD charge to maximize the conditioning effect seems to be determined by many factors such as the electrode material, the gap distance, and the electric circuit parameters [4].

Manuscript received on 17 September 2021, in final form 12 February 2022, accepted 17 April 2022. Corresponding author: N. Kita.

Basically, in conditioning process between electrodes in vacuum, defects on the cathode surface such as micro-protrusions are melted and removed by repetitive BDs. However, at the same time, micro-protrusions are generated on cathode surface by adhesion of melted anode material as particles [5, 6]. These anode-derived protrusions on the cathode can trigger BD and degrade the dielectric strength. Especially, large protrusions are disadvantageous for conditioning, because they may not completely removed by the subsequent BDs [5].

Conditioning effect cannot be expected with too little BD charge because the BD cannot remove the protrusions on the cathode sufficiently, but too much BD charge can damage the cathode. In order to realize the suitable control of BD charge, we need to consider the meltability and generated size of micro-protrusions.

In this paper, we focus on the anode-derived micro-protrusions generated by BDs in conditioning process. First, we conduct conditioning experiments on rod-plane Cu electrode system with several patterns of BD charge. After that, we observe the surface of rod cathodes with a digital microscope and measure the radii of protrusions. Then, we quantitatively consider the meltability of micro-protrusions. Next, we calculate the BD charge in the conditioning process and estimate a possible radius of anode-derived protrusion to be generated. From experimental and theoretical approaches, the size of protrusions generated in conditioning process is discussed. The effect of initial surface condition of the electrodes on the dielectric strength is also discussed.

2 EXPERIMENTAL SETUP AND PROCEDURE

Figure 1 shows the experimental setup and Figure 2 shows the electrode configuration. The electrodes were made of OFHC Cu with acid wash and heat treatment. The cathode surface roughness before experiments was less than 1 µm. The gap distance between the rod and plane electrode was 2 mm, and the tip radius of the rod electrode was 2 mm. We applied negative impulse voltage to the rod electrode in a vacuum chamber and conducted spark conditioning with up-down method. In the up-down method, the initial charged voltage of the impulse generator was 30 kV, and the charged voltage was increased by 10 kV steps. We considered that conditioning reached a saturation when the maximum BD voltage was not exceeded by next 300 times voltage application. The applied voltage and the discharge current were observed by a resistive-capacitive voltage divider (800 MΩ, 400 pF) and a current transformer (model 4997 by Pearson), respectively, and were recorded by a digital oscilloscope. The ratio of voltage divider is 1/2000. BD charge as the time integration of discharge current was controlled by a limiting resistor R_L of impulse generator: R_L = 20 kΩ, 11 kΩ, and 5 kΩ. The time of wave front (T_f) and the time of wave tail (T_t) of applied negative impulse voltage differed depending on the R_L. T_f/T_t = 19/94 µs for R_L = 20 kΩ, T_f/T_t = 12/78 µs for R_L = 11 kΩ, and T_f/T_t = 7.8/66 µs for R_L = 5 kΩ.

The vacuum pressure in the chamber was kept at the order of 10^{-6} Pa. Before and after these conditioning experiments, we observed rod electrode surfaces with a digital microscope. In the observation, we counted the number of visible protrusions and measured their radii.

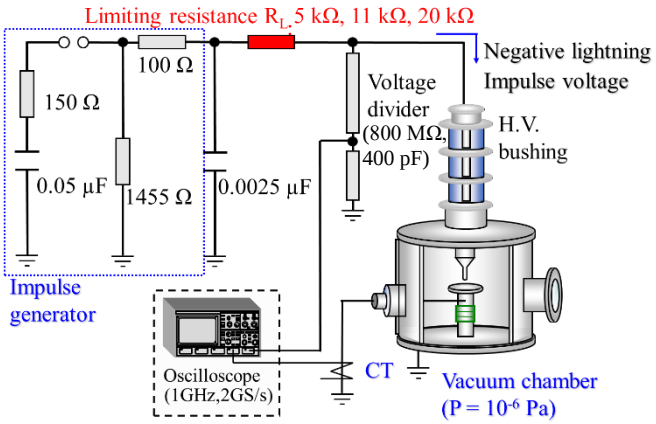

Figure 1. Experimental setup.

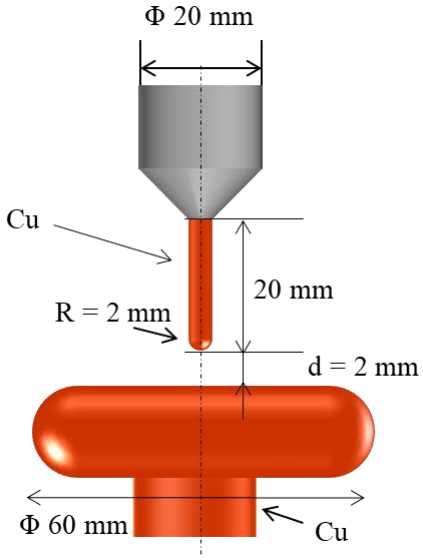

Figure 2. Configuration of rod-plane electrode system.

3 RESULTS AND DISCUSSION

3.1 CONDITIONING HISTORY AND CATHODE SURFACE BEFORE AND AFTER CONDITIONING

Figure 3 shows the conditioning histories for different BD charge at R_L = 20 kΩ, 11 kΩ, and 5 kΩ. The 50% BD voltage (V_{sat}) at conditioning saturation was V_{sat} = 141 kV for R_L = 20 kΩ, V_{sat} = 133 kV for R_L = 11 kΩ, and V_{sat} = 124 kV for R_L = 5 kΩ. Figure 4 shows the tip of each rod cathode surface before and after conditioning. Protrusions with the radius in the order of µm were not found before conditioning as shown in Figure 4a. After conditioning in the case of R_L = 20 kΩ and R_L = 11 kΩ, many protrusions with the radius of 1-10 µm were remained as shown in Figures 4b and 4c, where red circles denote the anode-derived protrusions. In contrast, after conditioning in the case of R_L = 5 kΩ, no protrusions were observed and the entire cathode surface was melted, where the protrusions generated during conditioning process seemed to be completely melted by BDs after conditioning saturation.

This article has been accepted for publication in IEEE Transactions on Dielectrics and Electrical Insulation. This is the author's version which has not been fully edited and content may change prior to final publication. Citation information: DOI 10.1109/TDEI.2022.3173493

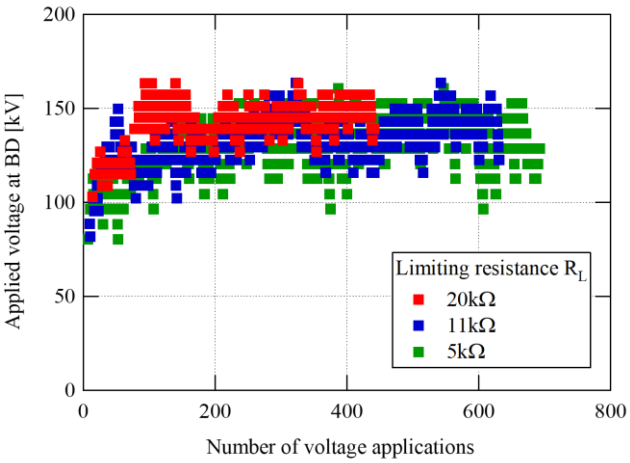

Figure 3. Conditioning histories.

3.2 MELTING OF MICRO-PROTRUSIONS BY BD

Meltability of micro-protrusions is important for conditioning effect, because conditioning is a process to remove the weak points on the electrodes by melting. Basically, during conditioning process, the original micro-protrusions existing on the cathode surface from the beginning are removed by BDs. In addition to this basic idea, we consider further phenomenon as shown in Figure 5. BD charge is injected into the anode, and a part of the anode can be melted. The melted anode material may adhere to the cathode surface to form new micro-protrusions as shown in Figure 5a. Then, the generated anode-derived protrusions in Figure 5a will be melted by the subsequent BDs as shown in Figure 5b. After this process is repeated, the conditioning can be saturated. When a residual surface shape or volume is formed, the improvement on cathode surface can be limited [5].

Here, we consider the mechanism for melting of protrusions in Figure 5b. Figure 6 shows an anode-derived protrusion shape which is one of the largest protrusions with the radius of about 12 μm on the cathode surface after conditioning saturation in the case of R_L = 11 kΩ. This trapezoidal shape is considered to be a residual shape of a micro-protrusion, melted by BDs through the conditioning process. Therefore, we assumed the generated anode-derived protrusion shape as the dotted curve in Figure 6, which is a quadratic curve approximated from the edge shape after conditioning.

We estimated the meltability of anode-derived protrusions by BD with the following procedure [5]. Bottom radius r corresponds to the size of a protrusion. We assumed that the protrusion has the similar quadratic shape as that of the dotted curve in Figure 6 for different r:

1. We divided the anode-derived protrusion into truncated cone parts (j = 1,…,N) in Figure 7 and calculated the electrical resistance R_j in each part. Each division was assumed to be a small cylinder, so we calculated R_j by the following equation:

$$R_j = \rho \frac{\Delta h}{S} \quad (1)$$

where ρ is copper resistivity, Δh is the height of small cylinder, and S is the cross-sectional area of small cylinder.

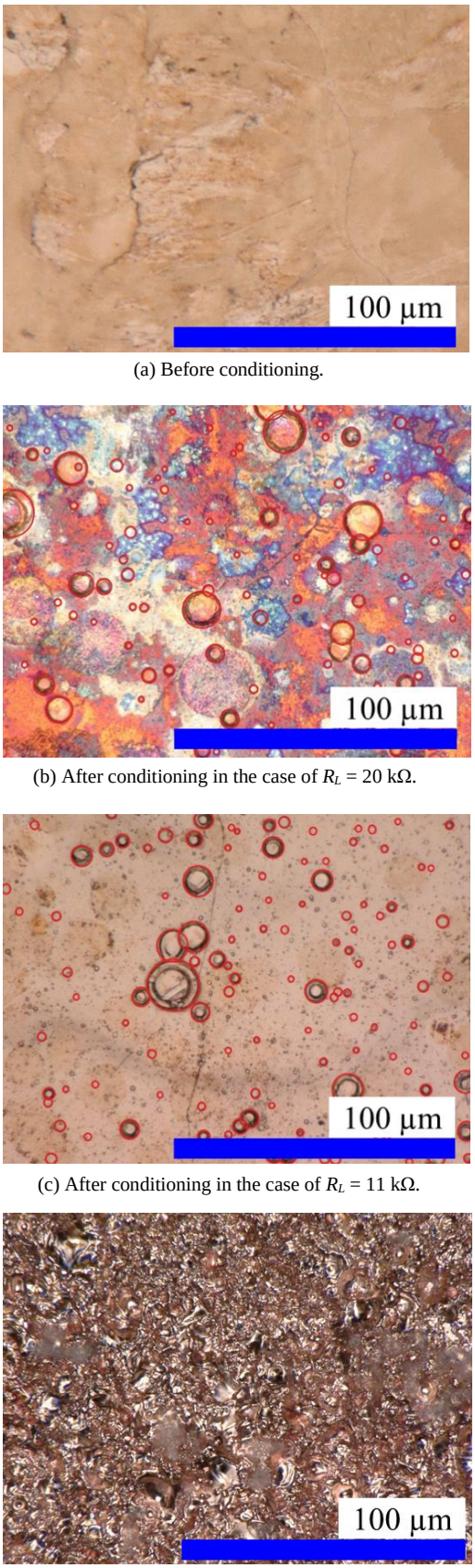

(a) Before conditioning.

(b) After conditioning in the case of R_L = 20 kΩ.

(c) After conditioning in the case of R_L = 11 kΩ.

(d) After conditioning in the case of R_L = 5 kΩ.

Figure 4. Rod cathode surface before and after conditioning. (Red circles are observed protrusions.)

2. We calculated the joule heat $R \cdot \int i^2 dt$ by the measured BD current i flowing through the electrical resistance in each part of the protrusion. An example of current and voltage waveforms is shown in Figure 8. In this estimation, we assumed that the current in each division flows uniformly on the horizontal surface without loss, and the averaged value of $\int i^2 dt = 0.30$ J/Ω was applied to all BDs. The standard deviation of $\int i^2\, dt$ in all BDs was 0.125 J/Ω.
3. We calculated the melting energy E_{melt} of the protrusion material Cu on the cathode per unit volume. E_{melt} is given by the following Equation:
$$E_{melt} = C(T_m - T_i) + H_f + H_e \quad (2)$$
where T_i is the initial temperature (27 °C) and the other material properties of Cu are listed in Table 1.
4. Meltable volume $V_{melt\_protrusion}$ is given by $R \cdot \int i^2 dt / E_{melt}$

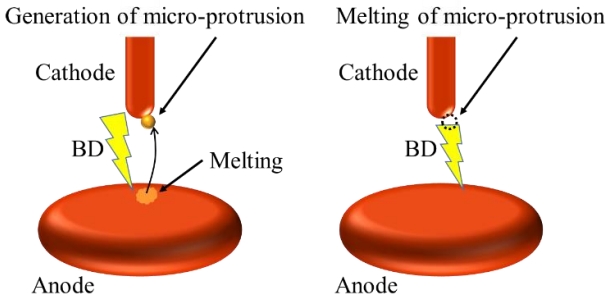

(a) Generation of micro-protrusion. (b) Melting of micro-protrusion.

Figure 5. Schematic illustration of generation and melting of micro-protrusion.

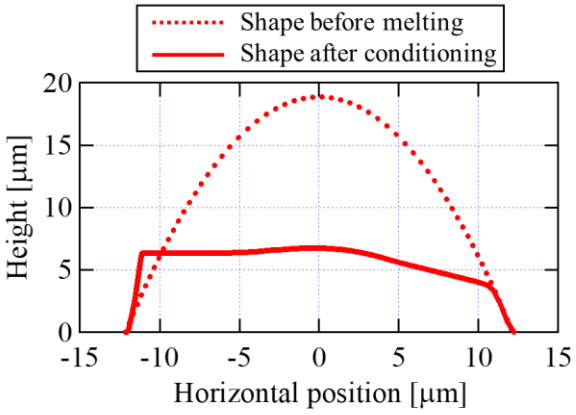

Figure 6. Protrusion shape observed on the cathode surface after conditioning for R_L = 11 kΩ.

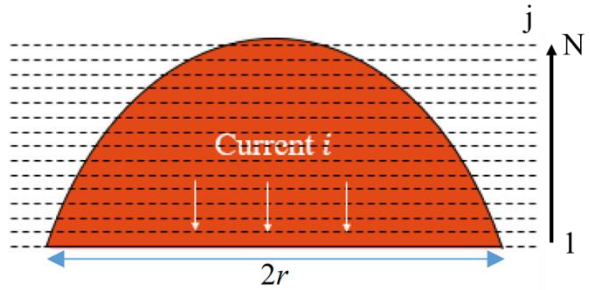

Figure 7. Division of a micro-protrusion into truncated cone parts.

Table 1. Material properties of copper.

Melting point T_m	1083.4 ℃
Heat capacity C	3.45×10^6 J/(m^3 · K)
Heat of fusion H_f	1.88×10^9 J/m^3
Heat of evaporation H_e	4.3×10^{10} J/m^3

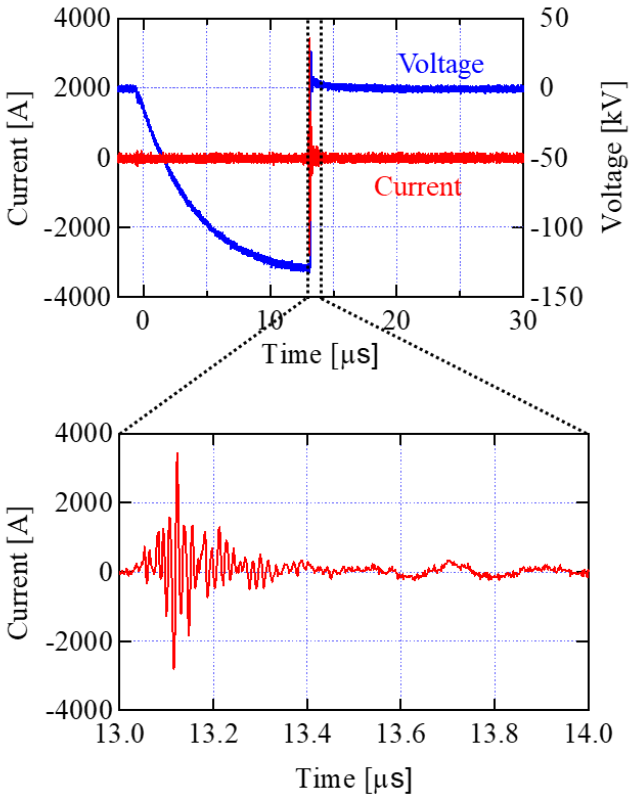

Figure 8. Example of measured current and voltage waveforms at BD (R_L = 11 kΩ, V = 133 kV).

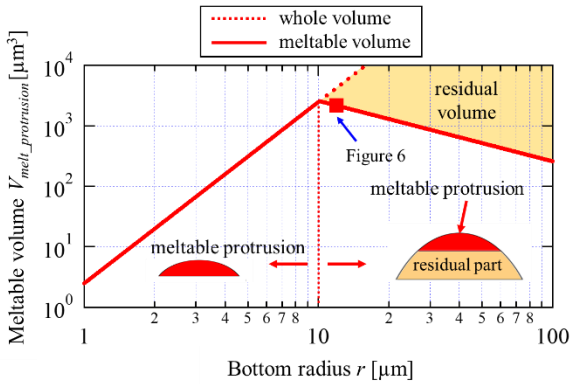

Figure 9. Meltable part and volume of protrusion for R_L = 11 kΩ.

Calculated relationship between meltable volume $V_{melt\_protrusion}$ and bottom radius r is shown as a solid line in Figure 9. The dotted line in Figure 9 shows the whole volume of protrusion as a function of bottom radius. Depending on the bottom radius r, Figure 9 can be divided into two parts, i.e. (a) r < 10 μm and (b) r > 10 μm.

(a) At r < 10 μm, the meltable volume $V_{melt\_protrusion}$ in the anode-derived protrusion is the same as the whole volume of the protrusion. It means that the whole protrusion can be melted by BD current.

(b) At r > 10 μm, the meltable volume $V_{melt\_protrusion}$ in the anode-derived protrusion is less than the whole volume of the protrusion. It means that only the tip part of protrusion can be melted, and bottom part remains unmelted through the conditioning process.

The dot (■) in Figure 9 represents the meltable volume $V_{melt\_protrusion}$ at r = 12 μm in Figure 6. The protrusions at r > 10 μm are estimated to remain on the cathode surface after conditioning. In these cases, the generation of micro-protrusions on cathode becomes an irreversible change to the cathode surface.

In spite of the residual protrusions after conditioning process, the improved BD voltage is maintained after the conditioning saturation as shown in Figure 3. However, an unfortunate generation of a larger protrusion may decrease the BD voltage, i.e. deconditioning.

3.3 GENERATION OF MICRO-PROTRUSIONS BY BD

In this section, we discuss the generation of anode-derived protrusions in Figure 5a. Many protrusions were observed after conditioning in Figures 4b and 4c. We counted the number of visible protrusions and measured their radii. After that, we compared the measured size with the estimated maximum size by meltable volume V_{melt_anode} of anode per a single BD.

3.3.1 SIZE OF MICRO-PROTRUSIONS

Figure 10 is the histogram of radius of anode-derived protrusions observed on cathode surfaces after conditioning, where the number of protrusions was counted in the pictures in Figure 4. It is clear that the smaller protrusions were more frequently observed. The maximum size was about 9 μm for R_L = 20 kΩ, and about 12 μm for R_L = 11 kΩ. It is suggested that the maximum size of protrusion is dependent on the BD charge, i.e. the larger maximum size of the protrusion is obtained with the higher BD charge for the lower R_L.

3.3.2 ESTIMATION OF BD CHARGE

For estimation of the maximum size of anode-derived protrusion, we need the BD charge Q_{BD} per a single BD. Therefore, we calculated the Q_{BD} at each BD in Figure 3, using the electric circuit simulation software PSCAD/EMTDC. Figure 11 shows the circuit model which describes the impulse voltage generator and BDs in the simulation tool. In Figure 11, 2.5 μH means the inductance of the line between the voltage divider and the vacuum gap. R means the arc resistance of the vacuum gap. We consider that R decays exponentially referring to the arc conductance model [7]. We assumed R as the following equation:

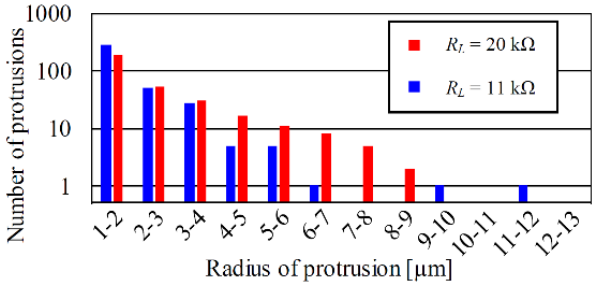

Figure 10. Measured radii of protrusions.

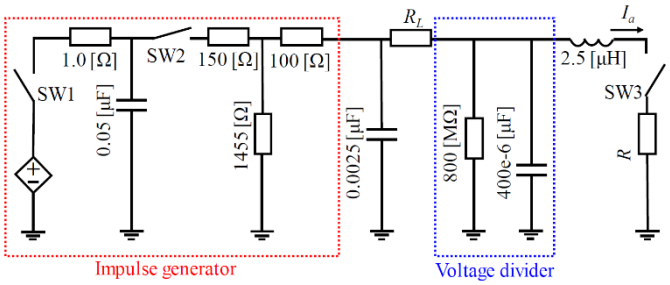

Figure 11. Simulation circuit in PSCAD/EMTDC.

$$R = R_0 exp\left\{-\frac{(t - t_{BD})}{\tau}\right\} \quad (3)$$

where R_0 is the resistance at the moment of BD, τ is time constant of resistance transition, and t_{BD} is time when BD occurs. Since BD is assumed to occur at the voltage peak in this paper, t_{BD} is the time when the voltage reached its peak. Each parameter in equation (3) is decided so that the simulated current waveform I_a is consistent with the measured waveform.

The simulation is carried out by the following procedure:

1. In the initial state, all switches SW1, SW2, and SW3 are off and capacitors are not charged.
2. The switch SW1 is turned on and the 0.05 μF capacitor is charged to the source voltage.
3. The switch SW1 is turned off and the switch SW2 is turned on to simulate the impulse voltage application.
4. The switch SW3 is turned on when the applied voltage reaches the peak value to simulate a BD of the vacuum gap.

For R_L = 20 kΩ, 11 kΩ, and 5 kΩ, we calculated the discharge current I_a. The BD charge Q_{BD} by a single BD is given by the time integration of I_a.

$$Q_{BD} = \int I_a dt \quad (4)$$

Figure 12 shows an example of current and voltage waveforms obtained by simulating BD in the above procedure 1～4. Table 2 shows Q_{BD} for R_L = 20 kΩ, 11 kΩ, 5 kΩ with the saturated voltage V_{sat}. In Section 3.2, we calculated $\int i^2 dt$ from the measured current waveform in Figure 8 to evaluate the meltability of the protrusions, where the $\int i^2 dt$ from the measured current waveform was the same order as that calculated from the simulated current waveform in Figure 12.

Table 2. V_{sat} and Q_{BD} for R_L = 20, 11, 5 kΩ.

Limiting resistance R_L [kΩ]	V_{sat} [kV]	BD charge Q_{BD} [mC]
20	141	0.351
11	133	0.528
5	124	0.912

This article has been accepted for publication in IEEE Transactions on Dielectrics and Electrical Insulation. This is the author's version which has not been fully edited and content may change prior to final publication. Citation information: DOI 10.1109/TDEI.2022.3173493

3.3.3 ESTIMATION OF MAXIMUM RADIUS OF PROTRUSION AND COMPARISON WITH MEASUREMENT RESULT

As mentioned in the introduction, there are two types of insulation weaknesses on the cathode: the original protrusions that exist on the cathode surface before conditioning and the anode-derived protrusions that are newly generated during the conditioning process. In a vacuum breakdown, a collision of ions into the anode accelerated by the anode sheath voltage is assumed to be the dominant energy input to the anode. The energy input E_{in} to anode is given by Equation (5).

$$E_{in} = \int U_{sheath} I_a dt \tag{5}$$

U_{sheath} is the anode sheath voltage and assumed to be constant at 1.5 V [8]. For the constant U_{sheath}, the meltable volume V_{melt_anode} of anode material is given by Equation (6). Here, the energy input to anode and the amount of meltable anode material are assumed to be proportional to Q_{BD}.

$$V_{melt\_anode} = E_{in}/E_{melt} = U_{sheath} Q_{BD}/E_{melt} \tag{6}$$

In Equation (6), E_{melt} is the amount of energy to melt the anode material per unit volume given by Equation (2).

We assumed the maximum radius r_{est} of anode-derived protrusions by Equation (7). This is the radius of sphere when the melted anode material with the volume of Equation (6) forms a single particle.

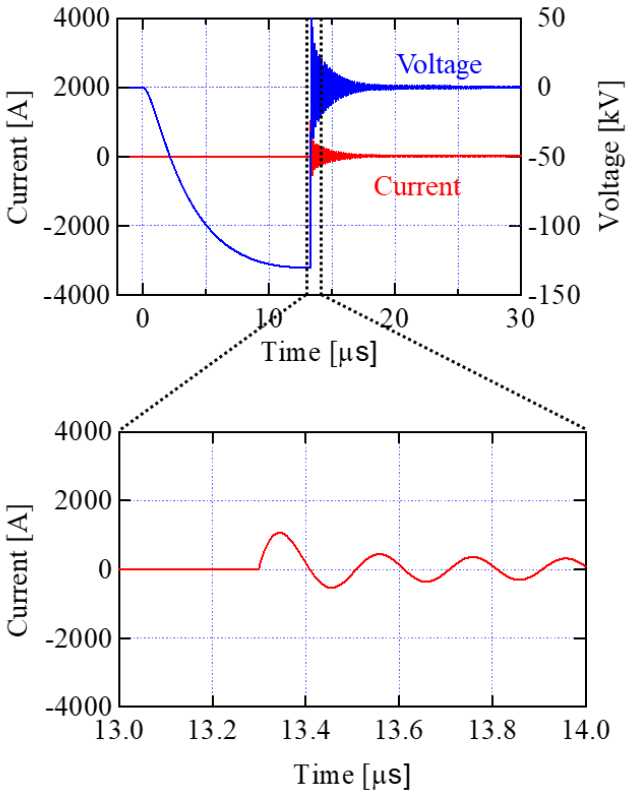

Figure 12. Example of simulated current and voltage waveforms at BD (R_L = 11 kΩ, V = 133 kV).

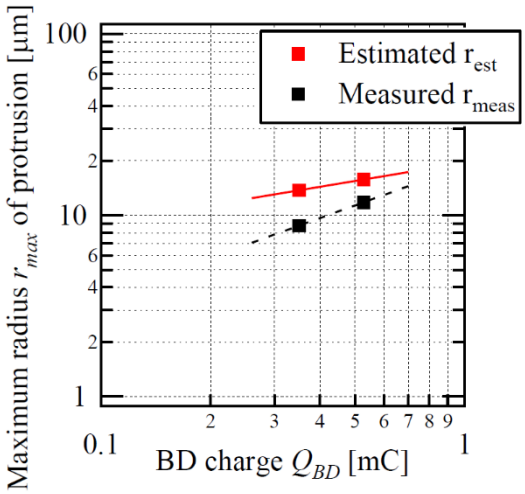

Figure 13. Estimated and measured radius of protrusion.

$$r_{est} = \left(\frac{3V_{melt\_anode}}{4\pi}\right)^{\frac{1}{3}} = \left(\frac{3U_{sheath}Q_{BD}}{4\pi E_{melt}}\right)^{\frac{1}{3}} \tag{7}$$

Equation (7) suggests that r_{est} is proportional to cube root of Q_{BD}. Calculation results of r_{est} with the maximum measured radii r_{meas} are represented in Figure 13. In Figure 13, r_{meas} is 8–12 μm, which is less than r_{est} of 13–16 μm. This difference may be attributed to the generation of two or more protrusions by a single BD, as the number of protrusions is greater than the number of BDs in conditioning experiments, and so on.

Basically, r_{meas} increases with Q_{BD}, because Equation (7) suggests that r_{est} increases with Q_{BD}. However, no protrusions were observed on the cathode surface after conditioning for R_L = 5 kΩ (Q_{BD} = 0.912 mC) in Figure 4d. We consider that $\int i^2 dt$ can determine the meltable volume $V_{melt\_protrusion}$ of anode-derived protrusions on the cathode in Figure 7. For R_L = 5 kΩ, BD current would be larger than those for R_L = 20 kΩ and 11 kΩ. In other words, since $\int i^2 dt$ is considerably large for R_L = 5 kΩ, most of the anode-derived protrusions were melted by joule heating at BD as shown in Figure 4d.

3.4 EFFECT OF ELECTRODE INITIAL SURFACE CONDITION ON DIELECTRIC STRENGTH

Figure 14 shows the relationship between V_{sat} and Q_{BD}. The black dotted curve is our previous research result [9], and the red dotted curve is this research result. The vertical error bars indicate the maximum and minimum BD voltage during the 300 voltage applications in conditioning saturation. Q_{BD} on the horizontal axis was estimated by the circuit analysis in Figure 11.

V_{sat} was higher at the smaller Q_{BD}. On the other hand, in our previous research with the same electrode system as in this research, V_{sat} had a maximum value at R_L = 5–7 kΩ (Q_{BD} = 0.6–0.8 mC) [9]. We discuss the cause of this difference in terms of Q_{BD} and the initial surface condition of electrode.

We used the electrodes with acid wash and heat treatment in this research, but the electrodes with no treatment were used in the previous research. No acid wash and heat treatment mean

This article has been accepted for publication in IEEE Transactions on Dielectrics and Electrical Insulation. This is the author's version which has not been fully edited and content may change prior to final publication. Citation information: DOI 10.1109/TDEI.2022.3173493

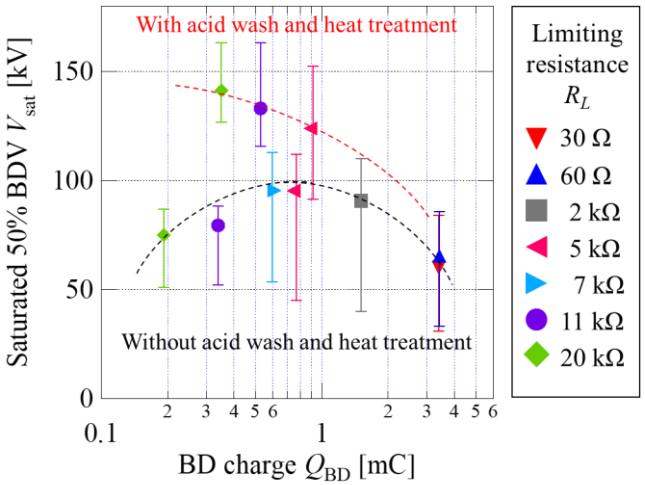

Figure 14. Relationship between V_{sat} and Q_{BD}.

that, if Q_{BD} is small (Q_{BD} < 0.4 mC), the initial weakness may not be removed by BDs. In another previous research [10], the conditioning characteristics depend on the initial surface condition of the electrode, if the Q_{BD} is small. In other words, V_{sat} with a good initial surface condition can be effectively increased even with a small Q_{BD} (Q_{BD} = 0.3–0.6 mC) as shown in Figure 14. Then, V_{sat} can be eventually limited by the generation of anode-derived protrusions on the cathode surface with the increased Q_{BD}.

On the other hand, if Q_{BD} is large (Q_{BD} > 2 mC), the deconditioning effect becomes dominant than the improvement effect on the electrode surface, and V_{sat} may decrease, regardless of the initial surface condition of the electrode.

From the above mechanism, the maximum V_{sat} may change depending on not only Q_{BD} but also the initial surface condition of the electrodes.

4 CONCLUSIONS

In this paper, we discussed the melting and generation mechanisms of micro-protrusions on cathode surface during spark conditioning in vacuum. Focusing on the breakdown charge Q_{BD} and initial surface condition of cathode, we discussed the relationship between saturation voltage V_{sat} and Q_{BD}. The main results are summarized as follows:

(1) We observed anode-derived micro-protrusions generated by material adhesion from anode to cathode in the conditioning process, and estimated the meltability of these anode-derived protrusions. Generation of anode-derived protrusions can be an irreversible change on cathode surface, when the generated anode-derived protrusions cannot be completely removed by the subsequent BDs.

(2) The maximum measured radius of anode-derived protrusions on the cathode surface after conditioning was 8–12 μm. The radius estimated by BD charge Q_{BD} was 13–16 μm and proportional to the cube root of Q_{BD}. The measured maximum radius was close to but did not exceed the estimated value, which implies the validity of such experimental and theoretical approach.

(3) In the case of small Q_{BD}, V_{sat} can be higher on the copper electrodes with acid wash and heat treatment than those with no treatment.

(4) In the case of large Q_{BD}, the deconditioning effect becomes dominant than the conditioning effect on the electrode surface, and V_{sat} may decrease, regardless of the initial surface condition of the electrode.

REFERENCES

[1] M. Honma *et al*, "History of vacuum circuit breakers and recent developments in Japan," IEEE Trans. Dielectr. Insul., vol. 13, no. 1, pp. 85-92, 2006.

[2] H. Okubo *et al*, "Advanced electrical insulation techniques for higher voltage vacuum interrupters," presented at the Cigre B3/D1 Colloquium, No. 218, 2013.

[3] "The Impact of the Application of Vacuum Switchgear at Transmission Voltage," Cigre Technical Brochure WG A3.27, 2014.

[4] H. Kojima *et al*, "Dependence of spark conditioning on breakdown charge and electrode material under a non-uniform electric field in vacuum," IEEE Trans. on Dielectrics and Electrical Insulation, vol. 23, no. 5, pp. 3224-3230, Jul. 2016.

[5] F. Kondo *et al*, "Suppression of conditioning effect in vacuum by micro-protrusions from anode," Int. Conf. on Electric Power Equipment-Switching Technology, 2019, pp. 467-471.

[6] S. Li *et al*, "Discharge and breakdown mechanism transition in the conditioning process between plane-plane copper electrodes in vacuum," IEEE Trans. Dielectr. Electr. Insul., vol. 26, no. 2, pp. 539-546, Apr. 2019.

[7] Y. Eshaf *et al*, "Simulation of Switching Arc Using Modified Mayr Arc Model," T. IEEJ, vol. 122-B, no. 1, pp.40-45, 2002.

[8] G. Ecker, "Anode spot instability 1. the homogeneous short gap instability," IEEE Trans. on Plasma Science, vol. PS-2, pp. 130-146, Sep. 1974.

[9] H. Kojima *et al*, "Controlling breakdown charge for conditioning procedure in vacuum under non-uniform electric field," presented at Int. Symp. on High Voltage Engineering, OD6-523, Buenos Aires, Argentina, Aug. 27-Sep. 1, 2017.

[10] H. Kojima *et al*, "Effect of initial electrode surface and breakdown charge on spark conditioning in vacuum under non-uniform electric field," Int. Symp. on Discharges and Electrical Insulation in Vacuum, 2018, vol. 1, pp. 51-54.

Naoki Kita (S'20) was born on 29 November in 1996. He received the BSc degree in Department of Electrical and Electronic Engineering from Kyushu Institute of Technology, Japan, in 2019, and the MSc degree in Department of Electrical Engineering from Nagoya University, Japan, in 2021. Currently, he is a Ph.D. candidate of Nagoya University at the Department of Electrical Engineering. He is a member of IEEJ.

Fuminori Kondo was born on 16 October in 1996. He received the MSc degree in Department of Electrical Engineering from Nagoya University, Japan, in 2020. Currently, he works at Hitachi Industrial Equipment Systems Corporation, Japan.

This article has been accepted for publication in IEEE Transactions on Dielectrics and Electrical Insulation. This is the author's version which has not been fully edited and content may change prior to final publication. Citation information: DOI 10.1109/TDEI.2022.3173493

Hiroki Kojima (M'11) was born on 7 December in 1975. He received his Ph.D. degree in 2004 in energy engineering and science from Nagoya University. He was a Researcher Fellow with the Japan Society for the Promotion of Science from 2000 to 2003. Since 2004, he has been at Nagoya University and presently he is an Associate Professor of Nagoya University in the Department of Electrical Engineering. Dr. Kojima is a member of IEEJ.

Naoki Hayakawa (M'90) was born on 9 September in 1962. He received his Ph.D. degree in 1991 in electrical engineering from Nagoya University. He has been at Nagoya University since 1990, where he is presently a professor in the Department of Electrical Engineering. From 2001 to 2002, he was a guest scientist at the Forschungszentrum Karlsruhe, Germany. Prof. Hayakawa is a member of IEEJ and CIGRE.

Hideaki Fukuda (M'16) was born on 26 December in 1988. He received the MSc degree in department of Electrical and Electronic Systems from Saitama University in 2013. He has been working at MEIDENSHA CORPORATION since 2013. Currently, he is engaged R&D of Vacuum Interrupters. He is a member of IEEJ.

Kenta Yamamura was born on 21 September in 1979. He received the MSc degree in Department of Applied Physics, School of Science and Engineering from Waseda University in 2004. He had been joined at Japan AE Power Systems Corporation in 2004 and transferred to MEIDENSHA CORPORATION in 2012. Currently, he is managed R&D of Vacuum Interrupters. He is a member of IEEJ.